Technical Report - MACKENZIE PRESBYTERIAN UNIVERSITY

Safety and Deflagration Tests of Lithium Batteries for Stationary Residential Use

Scope: This report presents a comparative evaluation of four lithium-ion battery technologies subjected to thermal, electrical, and fire-simulated stress conditions. The analysis documents the progression of thermal runaway, characterizing such as gas venting, flame development, and the occurrence of explosions.

Period: January 26
Data: January 7, 2026
Revision: 0
Report Language: English

Report Number: HU08

Summary

Disclaimer

This report serves as preliminary information intended for providing proof of the developed activities regarding the Huawei-Mackenzie Information Law project. The data and conclusions presented lack in depth revision and will be updated as all the acquired data is crossed and referenced in order to provide the best possible conclusions regarding the tests done to the selected devices.

1. Devices Under Test

To verify available ESS brands in the market in the residential battery market, 4 models were chosen, classified as A, B, C and D. Table 1 summarizes the Device Under Test (DUT) selected for this experiment.

Each battery was instrumented with temperature sensors to measure the battery temperature at different points, voltage sensors for cell-level monitoring and heat pads installed on the side of selected cells for thermal stress generation, along with a connection to one of the cells in the middle of the pack for electrical charge, in order generate electrical stress from overload in one of the battery cells.

Figure 1 presents an example of the cabling after the implementation of the heat pads, thermocouples and voltage measurement, yellow cables were used for the thermocouple's measurement, green for heat pad connection to external DC power supply and orange/black for voltage measurement. Also, Figures from 2 to 5 presents the batteries internal cell distribution diagram, with the location of heat pads, thermocouples, voltage measurement and indication of the overloadable cell.

Figure 1 – Cables for battery evaluation during tests.

Figure 2 – Cell distribution diagram for Battery A.

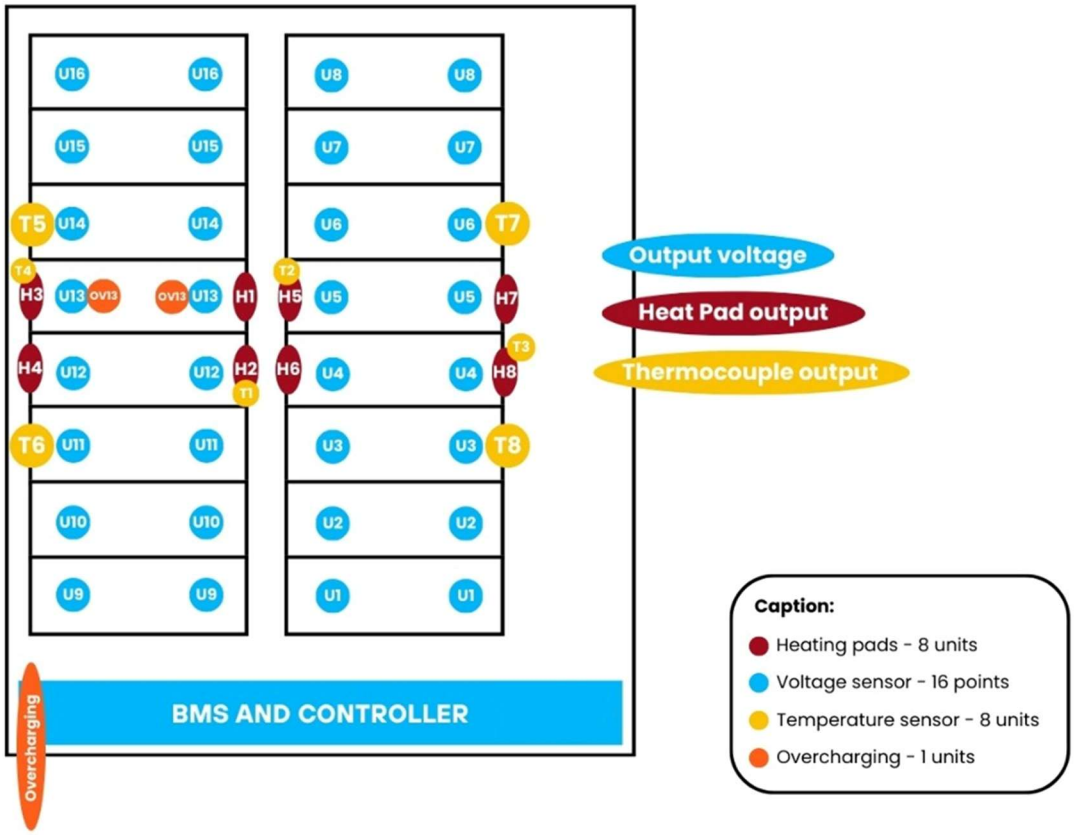

Figure 3 – Cell distribution diagram for Battery B.

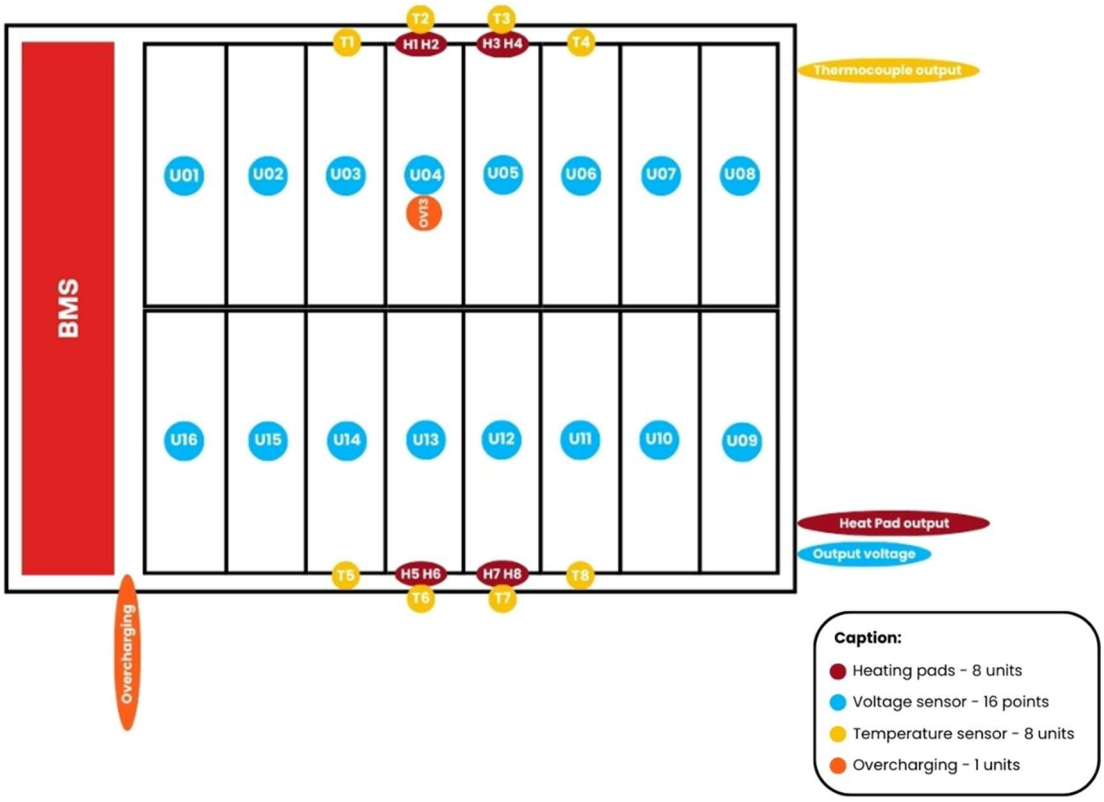

Figure 4 – Cell distribution diagram for Battery C.

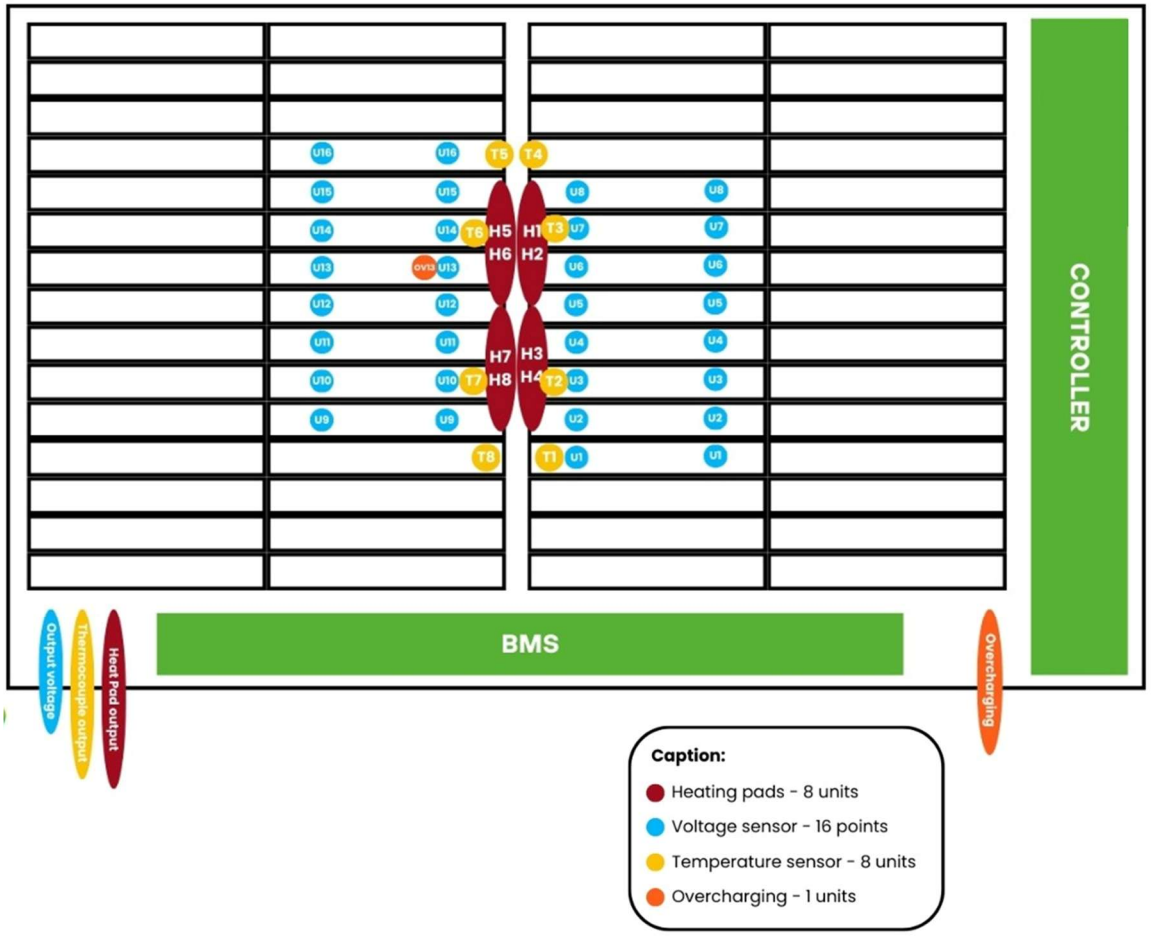

Figure 5 – Cell distribution diagram for Battery D.

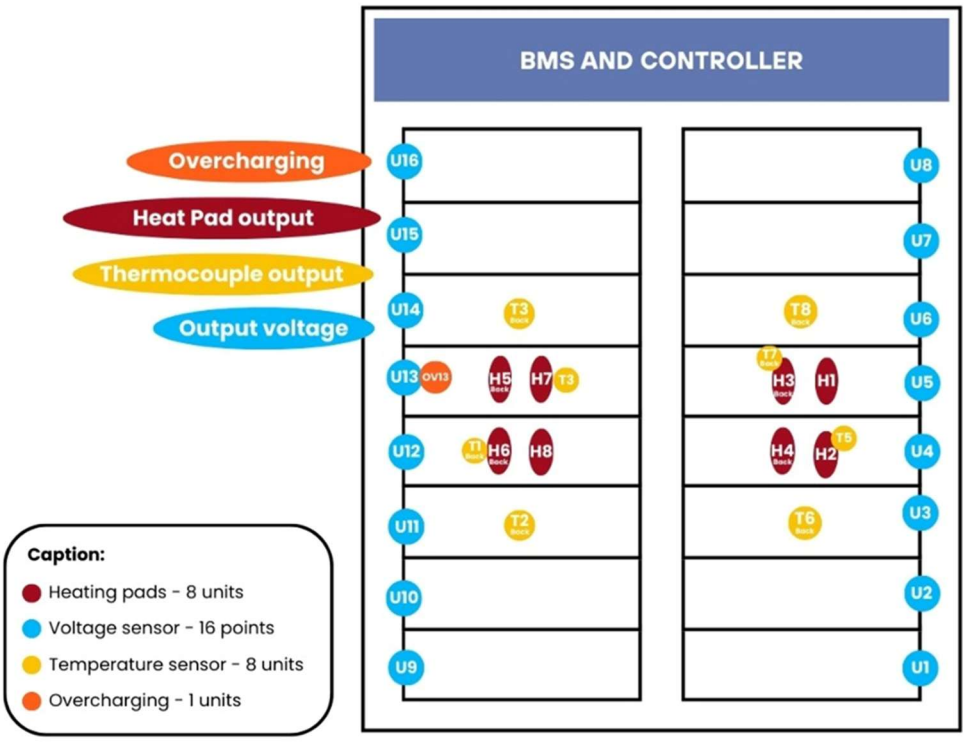

2. Tests on Battery A

On day one, Battery A was subjected to a controlled thermal stress regime with a total duration of 60 minutes. Figure 6 presents the behavior of the temperature curves recorded by the thermocouples, T1 to T8, during the final 37 minutes of this trial, allowing for the observation of the equipment's thermal behavior under adverse conditions.

Figure 6 – Thermal Monitoring of the Final 36 Minutes (Battery A – Day 1).

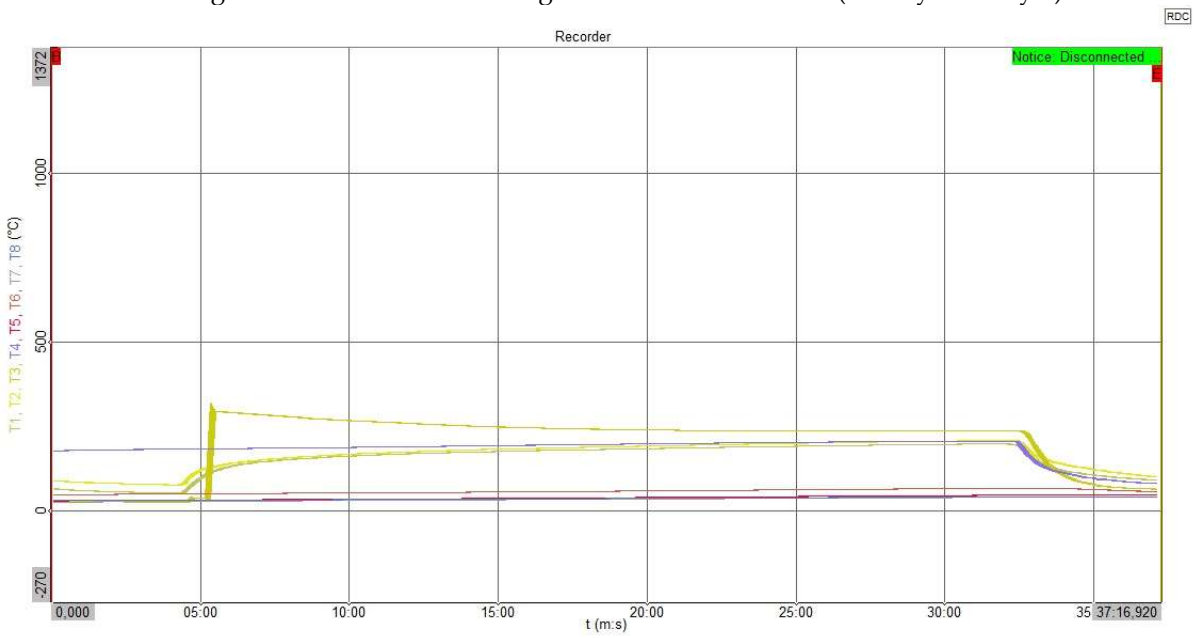

Analyzing the temperature curves in Figure 5, during the controlled thermal stress regime, it is observed that most sensors maintained stable temperature levels, remaining below 100°C. However, a specific thermal event is noted around the 5-minute mark, where 4 of the sensors indicated a temperature rise, where the T3 sensor reached a peak close to 300°C, which may indicate a thermal runaway event in the U4 battery cell.

The thermal stress was maintained for over 30 minutes after the temperature rise event, but due to operational issues, regarding the test facility operating hours, the thermal stress from the heat pads was ceased in order to finish the tests for day one. A gradual thermal dissipation near the 33-minute marks the time when the heat pads were turned off, with the thermal stabilization throughout the subsequent minutes. After verifying thermal stabilization inside battery, the test was ended for day one.

On day two, Battery A was subjected to a combined thermal and electrical stress regime to simulate critical operating conditions. The electrical stress was simulated with 17 A current injected directly in U13 battery cell. The thermal behavior of this test is detailed in Figure 7.

Figure 6: Thermal Runaway Monitoring (Battery A – Day 2).

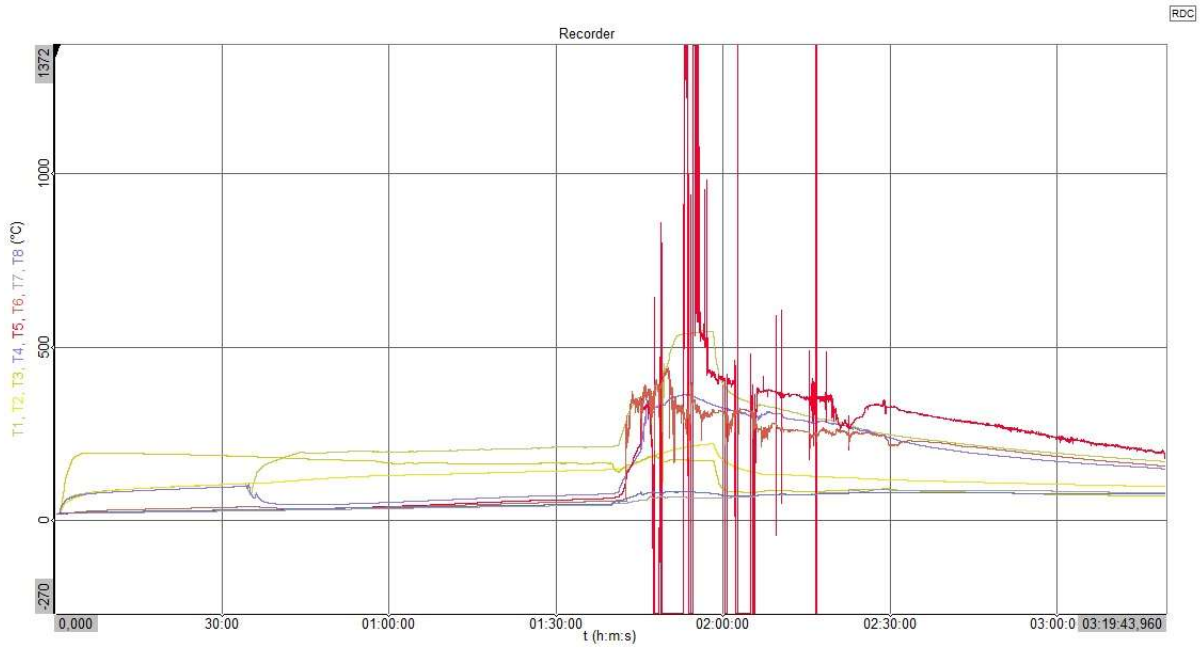

Differing from the behavior observed on day one, Figure 6 demonstrates that, after approximately 01:40:00 of testing under combined stress, the system entered thermal runaway. A vertical rise in the temperature curves is observed, with multiple sensors recording peaks that exceed the scale limit, above 1,300°C.

Figure 8 shows Battery A during the thermal runaway event. The flames on Battery A were started by the battery internal short-circuit, as indicated by audible arcing sounds during the events

.

Figure 8 – Visual Record of Thermal Runaway and Deflagration (Battery A).

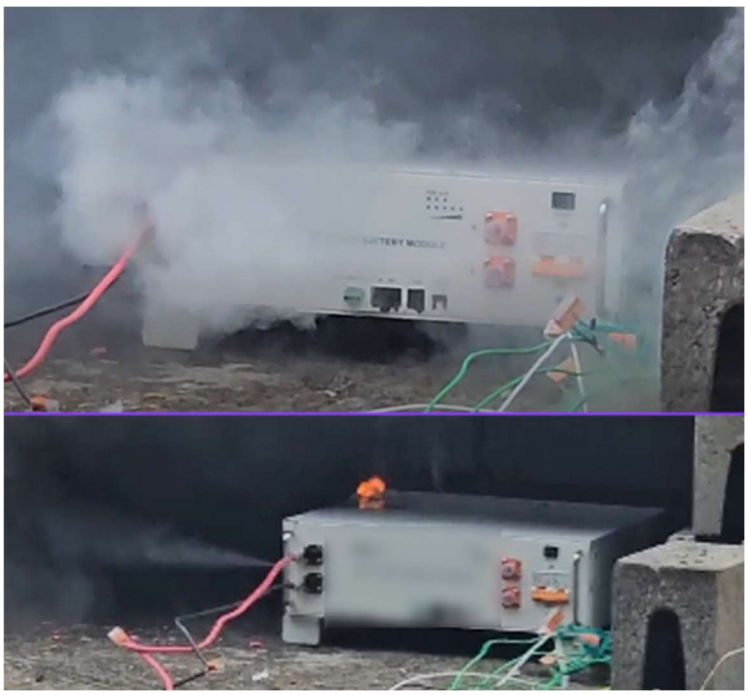

3. Tests on Battery B

On day two, Battery B was subjected to a prolonged cycle of thermal and electrical stress, totaling more than 02:40:00 of continuous monitoring.

The thermal behavior of this period is presented in Figure 9.

Figure 9: Stability Thermal Monitoring (Battery B – Day 2).

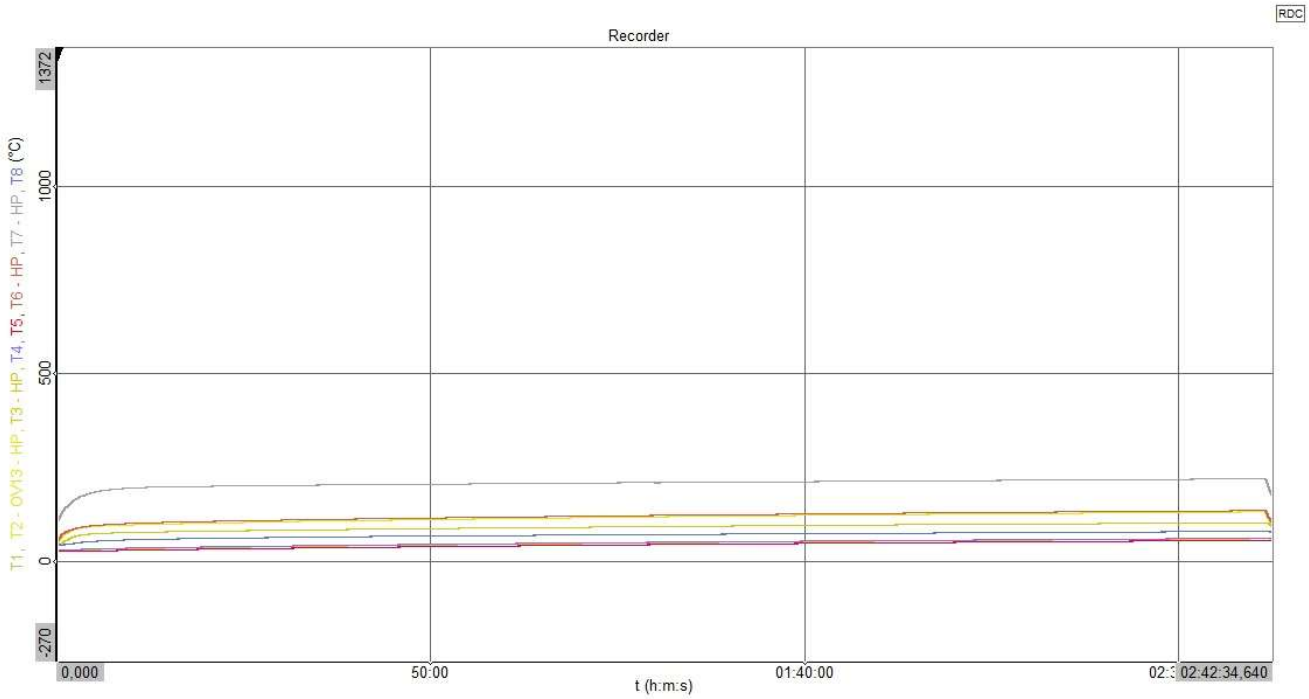

As evidenced in Figure 9, all temperature curves remained at controlled levels throughout the duration of the test. The highest temperature sensor recorded a stable level below 250°C, while the other sensors remained at lower levels.

Regarding the experimental results for Battery B, the unit maintained structural integrity throughout the preliminary thermal and electrical abuse tests.

On day three, Battery B was subjected to an external fire simulation regime to determine its structural collapse limit. The data captured in Figure 10 show the evolution of this scenario.

Figure 10: Thermal Runaway Record under Fire Simulation (Battery B – Day 3).

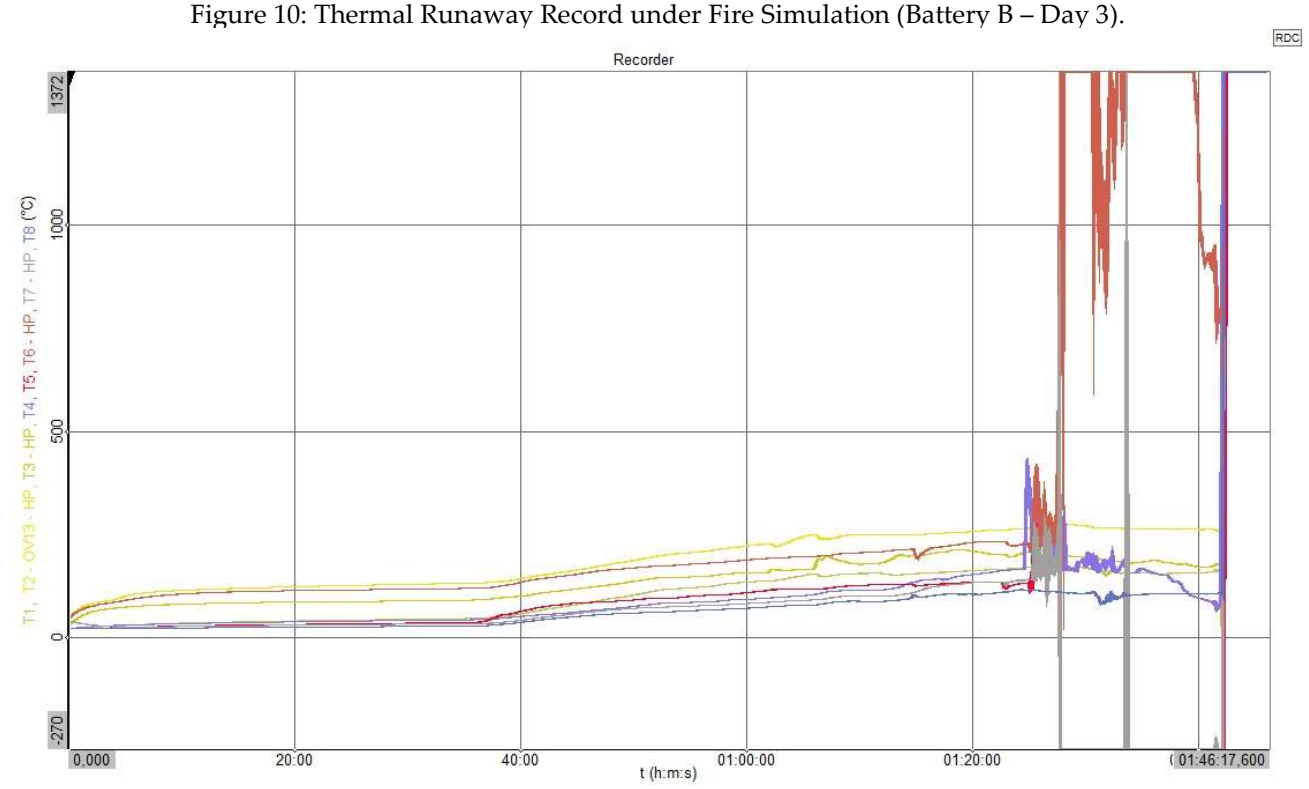

The analysis of Figure 10 reveals that stability was maintained for approximately 01:25:00 before the onset of instability. After this period, the thermal runaway is observed, characterized by temperature peaks that instantaneously exceeded the 1,300°C mark.

At the onset of thermal runaway, the unit initially exhibits smoke emission. Subsequently, flames are detected, which likely originated on the measuring cables due to proximity to the heat source. This fire was sustained by both the combustion of the cable materials and the continuous release of flammable gases from the battery, eventually resulting in the formation of a jet fire as gases were sprayed from battery.

Figure 11 shows the events during the first flames formation on Battery B.

Figure 11 – Visual sequence of smoke emission, flame onset on measuring cables, and jet fire formation (Battery B – Day 3).

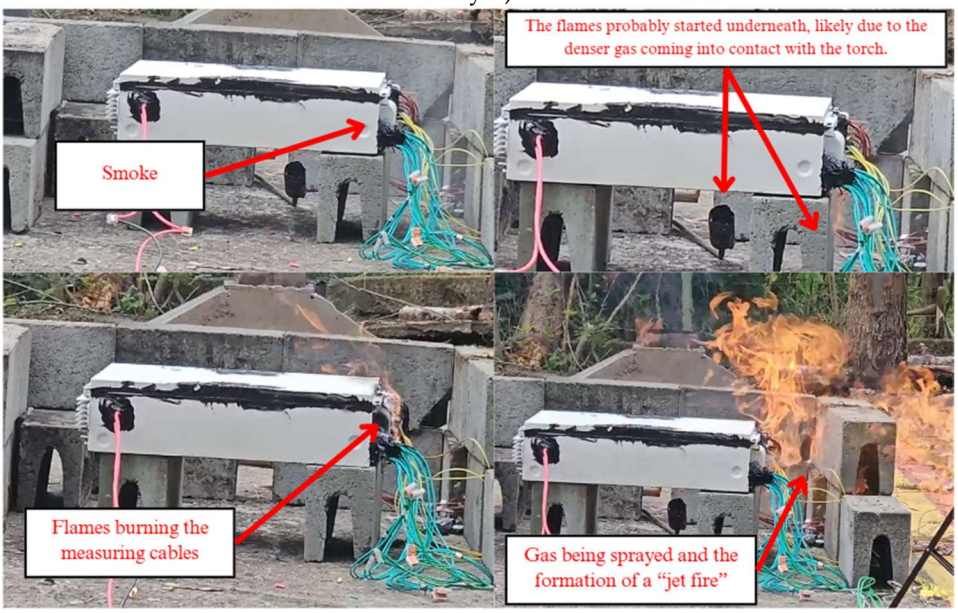

Complementing the visible spectrum observations, the infrared (IR) analysis in Figure 11 provides a thermal perspective of the probable fire induction in Battery B. While Figure 10 records the external appearance of smoke and flames, Figure 12 illustrates the heat localization during a one-second interval at the onset of the event.

The thermal imaging detects the heat from the external torch and its probable effect on the measuring cables and the area beneath the battery unit. This correlation between Figures 10 and 11 may confirm that the fire originates at the thermal hotspots identified on the cables and the base of the equipment before general flames develop.

Figure 12 – One-second sequence of Infrared camera recording during the onset of fire in Battery B.

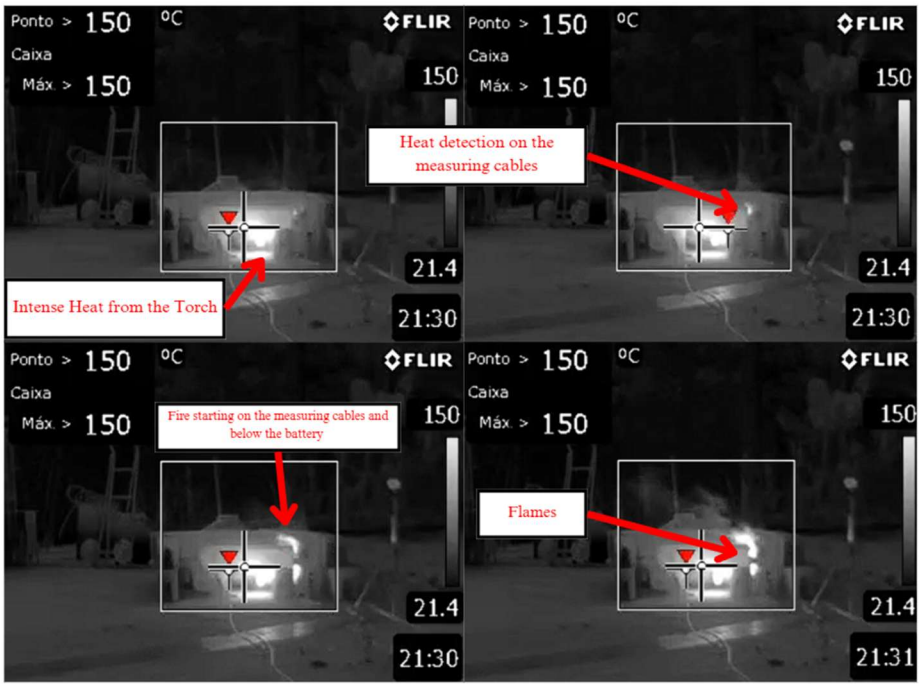

The thermal behavior during the only jet fire registered on Battery B is documented in Figure 13 via IR imaging where high-temperature flammable gases are expelled from the battery unit.

The IR signature shows a concentrated thermal plume extending horizontally from the battery.

Figure 13 – Infrared recording of the jet fire and gas expulsion phase (Battery B – Day 3).

Following the thermal runaway and subsequent deflagration of Battery B, a fire extinguisher was utilized to suppress the active flames. As documented in Figure 14, the fire did not reignite after the initial intervention. Following the suppression of the flames, a gradual and continuous reduction in smoke emission from the battery unit was recorded.

Figure 14 – Firefighter suppressing the fire using a extinguisher no Battery B.

4. Tests on Battery C

On day three, Battery C was subjected to an accelerated stress protocol, skipping the initial hour of only thermal abuse, combining simultaneous thermal and electrical stress from the start. During the initial phase of combined stress, it was observed that monitored cell number 13 may suffer a physical rupture, or opening, without, however, initiating the generalized thermal runaway phenomenon.

This initial behavior may be attributed to the lower energy density per cell battery C. However, when exposed to the external fire simulation, Battery C presented the fastest response among all units tested, reaching thermal runaway in 3 minutes of exposure.

The thermal monitoring of this event is detailed in Figure 15. Through the analysis of the curves, it is noted that, after the onset of instability, around 35 minutes into the total recording time, the temperatures escalated abruptly and uncontrollably.

Figure 15 - Deflagration Thermal Monitoring (Battery C – Day 3)

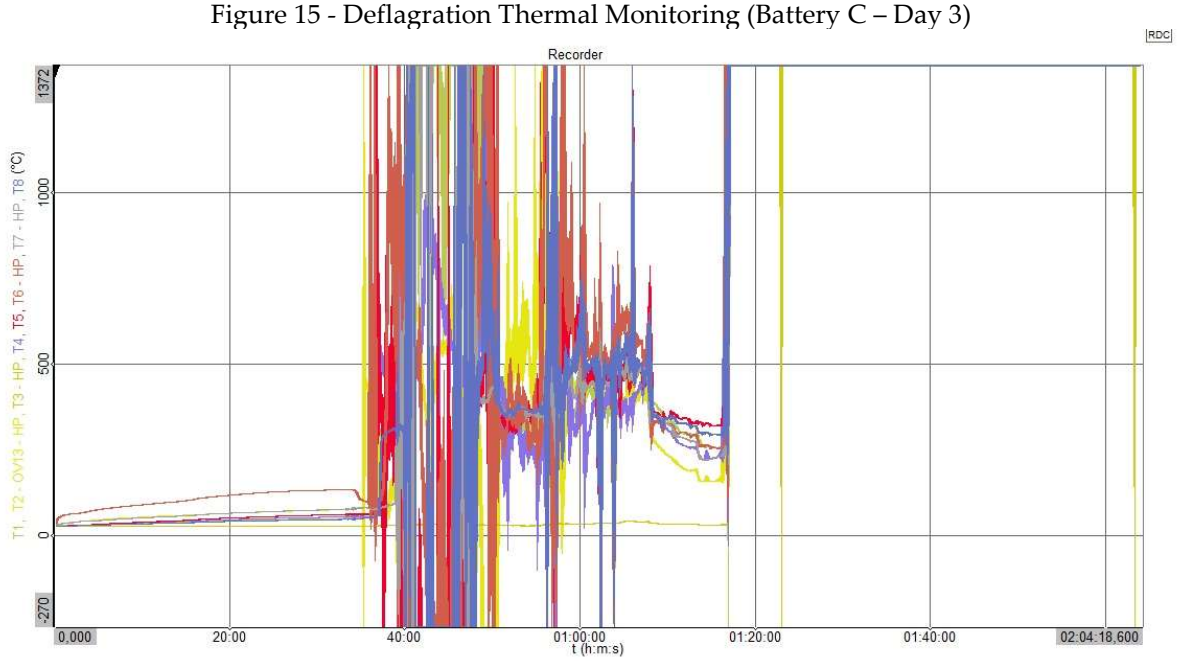

The sensors recorded thermal peaks that instantly exceeded 1,372°C, with violent oscillations indicating the successive destruction of the internal battery cells.

The test for Battery C during the fire simulation demonstrated a specific failure progression, documented in Figure 16. The event began with smoke emissions from the battery, indicating the start of internal cell venting. This was followed by a visible internal short-circuit, appearing as localized electrical arcing at the battery's edge.

As the short-circuit intensified, the interaction between the electrical sparks and the released battery gases may resulted in the ignition of sustained flames.

Figure 16 – Visual sequence of smoke emission, internal short-circuit, and subsequent ignition (Battery C – Day 3)

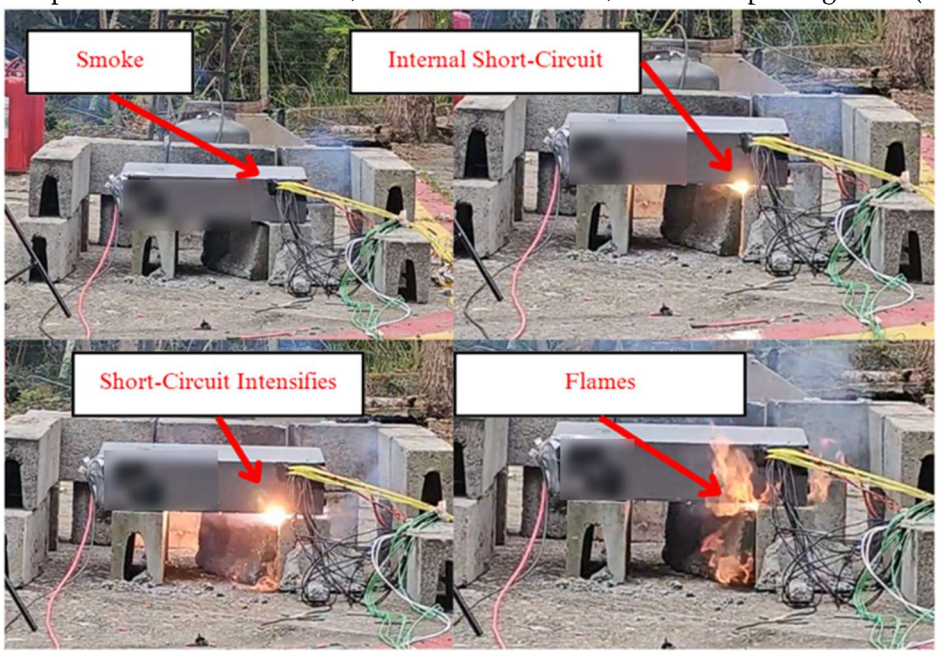

The progression of combustion in Battery C is documented in Figure 17, following the initial ignition phase. The Figure records the expansion of the flames across the external casing of the unit. During this stage, the fire reaches the measurement cables. The subsequent frames show the sustained burning of the instrumentation components as the fire intensifies.

Figure 17 – Progression of flames and impact on the measurement instrumentation (Battery C – Day 3).

Figure 18 documents the further progression of the thermal event in Battery C, where the combustion process intensifies. As the internal cells deteriorate, the unit exhibits a sequence of multiple explosions, these reactions are accompanied by sustained jet fires.

Figure 18 – Visual record of multiple explosions and jet fire (Battery C – Day 3)

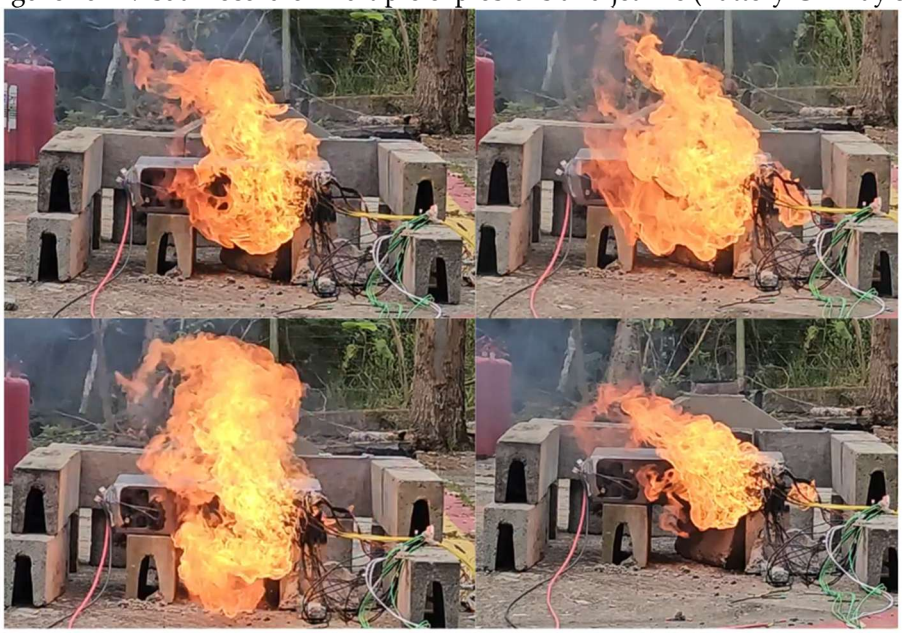

The sequence in Figure 19 documents the initial fire suppression attempt for Battery C using a fire extinguisher. The first intervention was unsuccessful in permanently extinguishing the flames. Following the initial discharge, the combustion intensified, and additional internal explosions were recorded within the battery.

Figure 19 – Initial fire suppression attempt on Battery C and subsequent intensification of flames and explosions.

As documented in Figure 20, the second fire suppression attempt successfully extinguished the visible flames on Battery C. Despite the extinction of the active fire, continuous smoke emission from the battery was recorded following the second intervention.

Figure 20 – Successful extinction of visible flames and subsequent continuous smoke emission (Battery C – Day 3).

As shown in Figure 21, a third intervention was performed by the firefighter with the objective of reducing smoke emission from Battery C. While a temporary decrease in emissions was recorded following this attempt, smoke production re-intensified after a brief period.

Figure 21 – Third intervention for smoke mitigation and subsequent re-intensification of emissions (Battery C – Day 3).

Figure 22 shows residual smoke emission persisted from Battery C following the third intervention. The left panel of the figure illustrates the intensity of the emissions remaining after previous suppression efforts. Consequently, a fourth intervention was initiated by the firefighter's team with the objective of further reducing the volume of smoke.

Figure 22 – Residual smoke emission after the third attempt (left) and the execution of a fourth mitigation intervention (right) (Battery C – Day 3).

Following the fourth suppression attempt, Figure 23 documents the subsequent behavior of Battery C. The upper panels of the figure illustrate a temporary reduction in smoke emission following the fourth intervention. However, after a brief interval, as shown in the lower panels, the emission of smoke re-intensified.

Figure 23 – Observation of temporary smoke reduction (top) followed by re-intensification (bottom) after the fourth suppression attempt (Battery C – Day 3).

Figure 24 documents the fifth intervention, performed by the firefighter with the objective of cooling Battery C to facilitate its safe removal and transport the unit to a separate location for stabilization. In this designated area, foam was utilized to complete the cooling process and ensure the termination of internal exothermic reactions.

Figure 24 – Fifth intervention for removal of Battery C (Battery C – Day 3).

5. Tests on Battery D

At the end of the third day of trials, Battery D was subjected exclusively to the external fire simulation protocol, without going through previous stages of isolated thermal or electrical stress.

The thermal behavior of battery D is presented in Figure 25. It is observed that Battery D showed higher thermal resistance than battery C, yet slightly lower than Battery B, maintaining thermal integrity for approximately 65 minutes before transitioning to the critical state. The sensors recorded peaks that instantaneously exceeded the 1,372°C.

Figure 25 – Thermal Monitoring of Battery D – Fire Simulation.

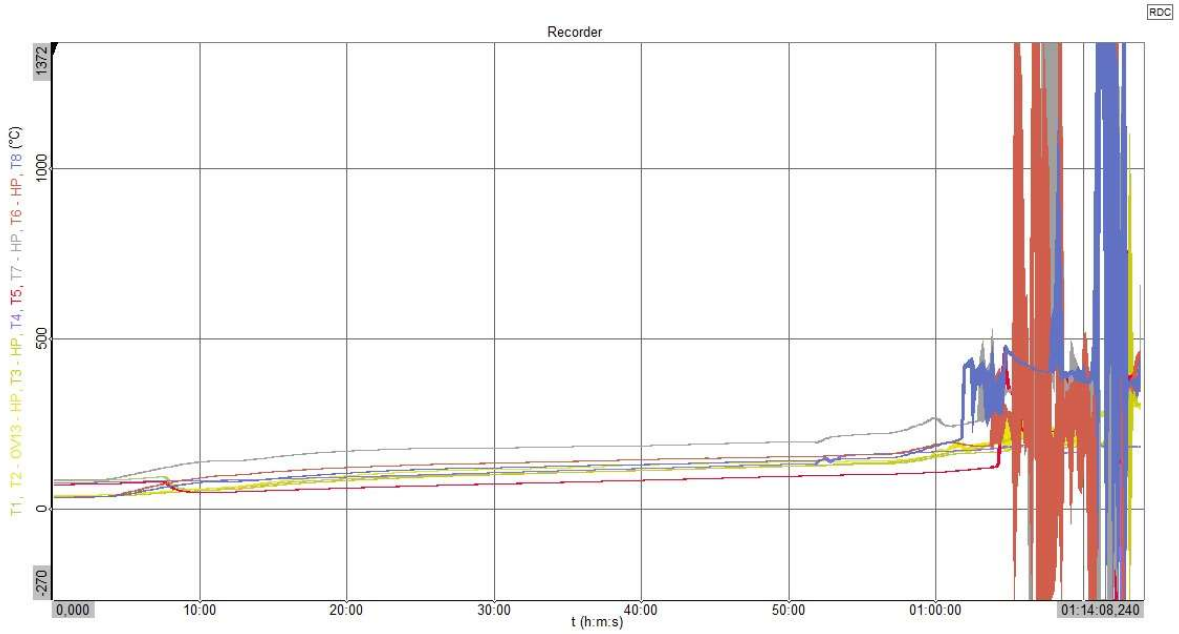

Battery D maintained its structural integrity for approximately 65 minutes before entering the state of thermal runaway, the equipment exhibited a sequence of explosions and jet-fire. Based on comparative observations during the POC, these events demonstrated the highest intensity among all tested units, characterized by rapid energy release and the formation of large-scale flames, figure 26 shows multiples explosions recorded.

Figure 26 – Visual record of high-intensity explosions and jet-fire (Battery D – Day 3)

The infrared recording in Figure 27 documents thermal behavior during the deflagration of Battery D. The imaging captures varius explosions plumes at different intervals.

Figure 27 – Infrared monitoring of the deflagration phase (Battery D – Day 3)

Figure 28 shows the active fire in Battery D was successfully suppressed during the initial intervention by the firefighter and did not reignite. However, the high volume of smoke emission following the extinction of visible flames necessitated multiple subsequent interventions for mitigation. This requirement for repeated suppression attempts to manage persistent gas and smoke release mirrors the behavior previously observed during the tests for Battery C.

Figure 28 – Successful initial fire suppression and subsequent interventions for smoke mitigation (Battery D – Day 3).

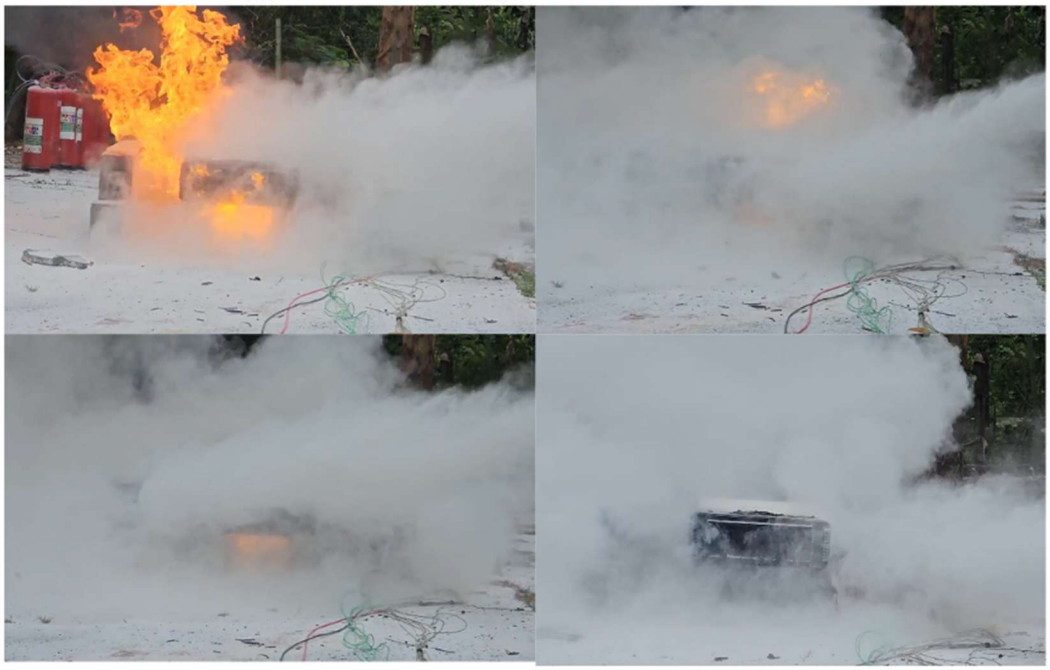

6. Preliminary Conclusions

Based on the experimental results, the preliminary conclusions indicate distinct thermal degradation behaviors and resistance thresholds among the analyzed units. Battery B demonstrated the highest resistance duration prior to

the onset of thermal runaway, with the active fire successfully suppressed in a single intervention without subsequent reignition. Battery A underwent deflagration prior to the official fire simulation stage, a behavior not observed in Battery B, which maintained its structural integrity under the same applied stress.

In contrast, Batteries C and D presented more complex failure modes and greater suppression challenges. Battery C required five separate interventions due to the persistence of flammable gas emissions and internal explosions that occurred following the initial extinction of visible flames. While Battery D maintained structural integrity for approximately 65 minutes, it recorded the most violent explosions and highest-intensity jet-fire among all tested samples. Furthermore, Battery D required multiple subsequent interventions for smoke mitigation after the active fire was extinguished, mirroring the behavior observed in Battery C.

The preliminary experimental data and the comparative analysis of the occurrence and intensity of thermal runaway for all tested batteries are summarized in Table 2.

Table 2: Summary of Observed Events Intensity

Battery	**Thermal and Electric Abuse Resistance**	**Smoke Emission**	**Internal Short-Circuit**	**Active Fire**	**Explosions**	**Jet Fire**	**Fire Suppression Difficulty**
A	Medium	Moderate	Observed	Moderate	Observed	Observed	N/A
B	High	Moderate	Not Observed	Moderate	One Event observed	One Event observed	Low
C	Low	High	Observed	High Intensity	Multiple events	Multiple events	High
D	N/A	High	Not Observed	Highest Intensity	Multiple violent events	Multiple violent events	High

These are the final considerations of the report.

São Paulo, January 7, 2026.

Bruno Luis Soares de Lima, PhD.
bruno.lima@mackenzie.br

José César de Souza Almeida Neto, PhD.
jose.almeida@mackenzie.br